ARTICLE

Check for updates

Higher vegetation sensitivity to meteorological drought in autumn than spring across European biomes

Hongxiao Jin [1✉], Sergio M. Vicente-Serrano [2], Feng Tian [3], Zhanzhang Cai[1], Tobias Conradt[4], Boris Boincean[5], Conor Murphy [6], Begoña Alvarez Farizo[2], Sam Grainger[6], Juan I. López-Moreno [2] & Lars Eklundh[1]

Europe has experienced severe drought events in recent decades, posing challenges to understand vegetation responses due to diverse vegetation distribution, varying growth stages, different drought characteristics, and concurrent hydroclimatic factors. To analyze vegetation response to meteorological drought, we employed multiple vegetation indicators across European biomes. Our findings reveal that vegetation sensitivity to drought increases as the canopy develops throughout the year, with sensitivities from −0.01 in spring to 0.28 in autumn and drought-susceptible areas from 18.5 to 57.8% in Europe. Soil water shortage exacerbates vegetation-drought sensitivity temporally, while its spatial impact is limited. Vegetation-drought sensitivity strongly correlates with vapor pressure deficit and partially with atmospheric CO_2 concentration. These results highlight the spatiotemporal variations in vegetation-drought sensitivities and the influence of hydroclimatic factors. The findings enhance our understanding of vegetation response to drought and the impact of concurrent hydroclimatic factors, providing valuable sub-seasonal information for water management and drought preparedness.

[1] Department of Physical Geography and Ecosystem Science, Lund University, Lund, Sweden. [2] Instituto Pirenaico de Ecología, Consejo Superior de Investigaciones Científicas (IPE-CSIC), Zaragoza, Spain. [3] Hubei Key Laboratory of Quantitative Remote Sensing of Land and Atmosphere, School of Remote Sensing and Information Engineering, Wuhan University, Wuhan, China. [4] Potsdam Institute for Climate Impact Research, Potsdam, Germany. [5] Selectia Research Institute of Field Crops, Bălţi, Moldova. [6] Irish Climate Analysis and Research UnitS (ICARUS), Department of Geography, Maynooth University, Co, Kildare, Ireland. ✉email: hongxiao.jin@nateko.lu.se

Droughts are periods of lower than long-term average water availability[1]. Climate change is leading to increased intensity, duration, and frequency of droughts in certain regions of the world[2,3], which negatively impacts both societies and ecosystems[4,5]. Drought can decrease vegetation productivity[6], change vegetation composition[7], decrease biodiversity[8,9], and reduce ecosystem services[5]. Many European countries have suffered from severe summer droughts in the last decades[10–12]. In Europe and the UK, the average annual economic loss due to drought during 1981–2010 was about 9 billion euros, with half of these losses being from agriculture[13,14], highlighting the importance of preparedness and knowledge of vegetation responses to drought.

Meteorological droughts, caused by precipitation deficit, have complex effects on vegetation growth that are influenced by multiple hydroclimatic factors. Here, "growth" refers to vegetation processes that result in changes in biomass or primary production in a broad sense[15]. The hydroclimatic factors include soil water availability (soil moisture, SM), transient atmospheric dryness (vapor pressure deficit, VPD), solar radiation (net radiation, R_n), and atmospheric carbon dioxide (aCO_2) concentration[16–19]. These factors can interact in ways that either amplify or mitigate the impacts of drought on biophysical processes. Vegetation response to meteorological drought depends on whether its growth is limited by water (SM) or energy (R_n)[17]. Whereas the relative roles of SM and VPD on vegetation during drought are challenging to disentangle[20]. Also, the aCO_2 effect during vegetation water stress remains debated[21] and is intertwined with other factors[22]. A comprehensive study is needed to assess the relative roles of these factors on vegetation growth and responses to drought, attaining a holistic understanding of the interplay among various concurrent factors with meteorological drought.

The Standardized Precipitation and Evapotranspiration Index (SPEI)[23] is often used to estimate characteristics of meteorological drought events, including drought severity, intensity, and duration; for a detailed definition, see ref. 24. The SPEI takes into account the water balance between precipitation and atmospheric evaporative water demand and provides a comprehensive understanding of the water stress conditions on vegetation at global and regional scales[25–28]. SPEI has been shown to outperform other indices in evaluating drought impacts on soil moisture, vegetation activities, crop yield and forest growth[29–31]. The SPEI calculated from coarse climate data (0.5-degree) has been used to assess the impacts of interannual variability of SPEI on vegetation activities over global and regional scales[32,33]. Recently developed high-resolution (0.1-degree) climate reanalysis data offer the potential for assessing drought impacts on vegetation using SPEI with spatially detailed information.

Drought can happen at any time of a year[34,35], and the vegetation responses to drought vary depending on the timing of drought and vegetation growing stage due to varying water requirements along seasonal vegetation growth[36–38]. Current research has primarily focused on the overall annual vegetation response to drought and its time-scale effects[32], post-drought recovery[36], and the impacts of drought on vegetation phenology[39]. The fundamental knowledge about immediate sub-seasonal vegetation responses to drought over large scales has been overlooked. This information is crucial for ecosystem drought monitoring[40], as many studies on plant drought stress responses have been limited to pot-scale experiments[41]. The extent to which vegetation sub-seasonal growth is affected by drought at the ecosystem scale remains unclear, as the applicability of Liebig's law of the minimum may not extend from the individual to the community level[42,43]. The situation is complicated by the spatial variability of soil water availability preceding

meteorological droughts, in addition to other factors necessary to meet the minimum growth requirements of individual plants[44]. The knowledge of sub-seasonal vegetation responses to water availability is needed for crop planning, efficient water resource management, optimizing ecosystem restoration, and mitigating drought risks.

Europe experienced drying conditions in the south and wetting conditions in the north, with a tendency towards wetter winters and drier summers during past decades[34]. The region of Europe facing water stress has been projected to increase significantly everywhere[45]. Several studies have analyzed the effects of drought on pan-European vegetation using remotely sensed vegetation proxies. For example, the Normalized Difference Vegetation Index (NDVI) was used and revealed that drought led to decreased vegetation production in central Europe during 1999–2010[46]. Another closely related indicator, the fraction of photosynthetically active radiation (FPAR), was also employed, and it found that vegetation in northern Europe showed a weaker sensitivity to drought compared to vegetation in southern Europe during the period 1982–2011 and that droughts had limited impacts on boreal and alpine forests but significantly reduced productivity in agricultural regions[47]. In a comparison study of European drought during 2001–2015 using an ensemble of satellite-derived land surface products and carbon cycle models[48], it was reported that NDVI failed to capture drought impacts on vegetation. A single vegetation proxy, e.g., the greenness proxy NDVI, only provides one facet related to vegetation growth and may be insufficient to understand vegetation responses to environments[49]. Some vegetation indicators from satellite observation also have limitations, such as the issues caused by snow cover and dense vegetation[50], leading to potential inaccuracy in the estimation of vegetation growth. A comprehensive assessment of vegetation responses to drought requires evaluating multiple indicators, including greenness, structure, physiology, photosynthetic light absorption, productivity, and more, to offer a complete understanding of vegetation's response to drought stress.

Taking into account the multifaceted nature of plant growth[15], this study uses an ensemble of remotely sensed vegetation indicators in combination with a state-of-the-art gridded climate dataset to investigate how vegetation responds to drought across European biomes during 2000–2020. We assess the immediate impacts of interannual variability of SPEI on vegetation at a half-month step during canopy development over a year, considering different time scales of drought, including both positive values for wet and negative values for dry conditions. The robust statistical methods are used to classify drought-vegetation associations and disentangle meteorological drought impacts on vegetation growth from concurrent hydroclimatic factors, including SM, R_n, VPD, and aCO_2, at each growing stage. We examine vegetation responses to drought separately for the most common European land cover types.

Results

Vegetation-drought association. Vegetation growth was correlated to drought with varying strengths at different drought time scales in different months of the year across European biomes. The correlation values between the ensemble vegetation indicators and SPEI are summarized in Fig. 1 for three typical months of a vegetation season (spring onset, summer peak, and autumn senescence). During the spring months of vegetation growth onset, 18.5% of the area presented a significant positive correlation (implying vegetation susceptible to drought) between vegetation and SPEI, whereas 26.5% of the area had significant negative correlation, leading to an average correlation coefficient
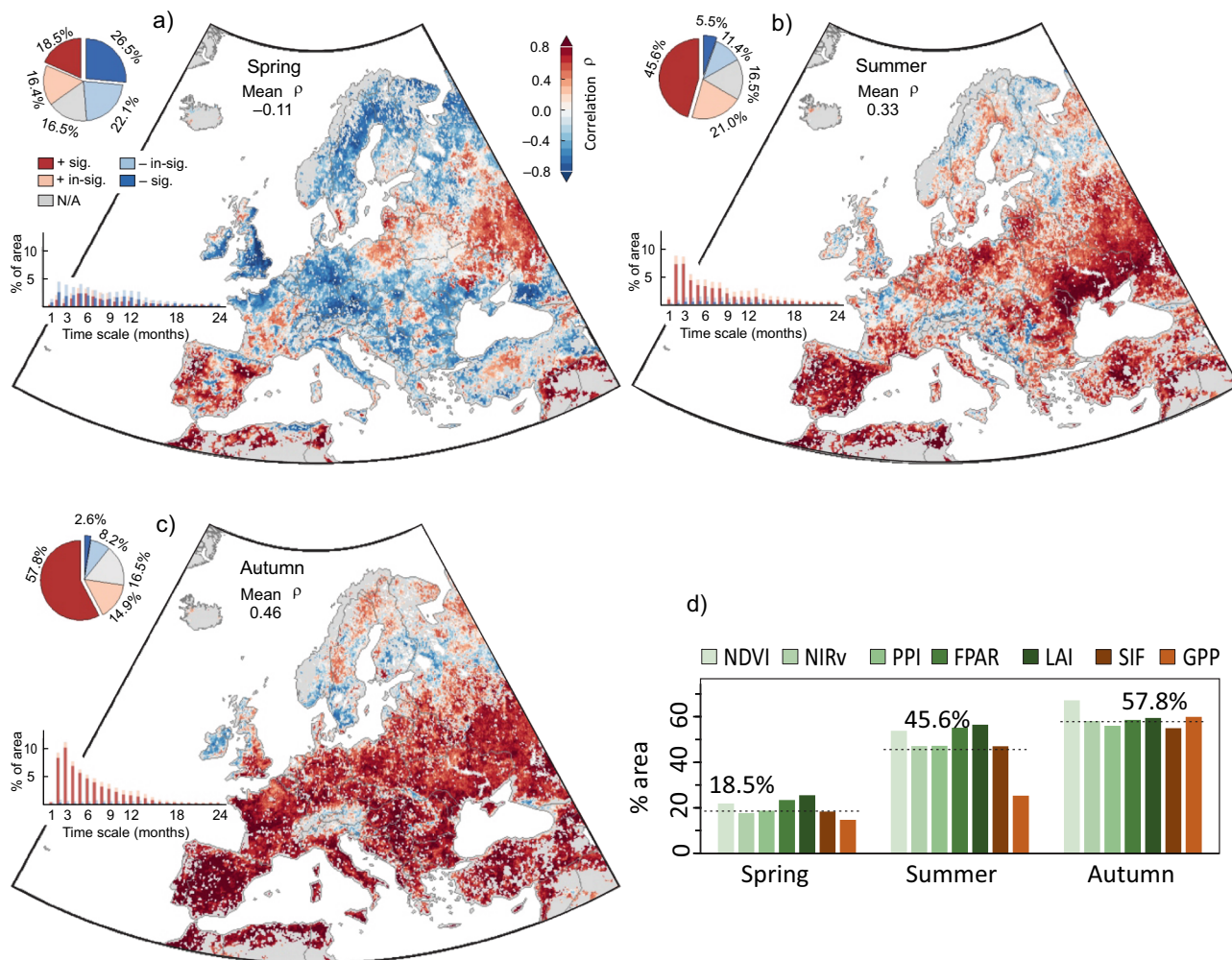
Fig. 1 Maps of vegetation-drought Spearman correlations during three vegetation seasons. a Spring months of growth onset, **b** summer months of peak growth and **c** autumn months of senescence, determined from an ensemble of seven vegetation indicators (NDVI, NIRv, PPI, FPAR, LAI, SIF, and GPP) and drought index SPEI. **d** Bar chart of the proportion of drought-susceptible areas with significant positive correlations between vegetation and SPEI in three vegetation seasons. The dot-dash lines denote the ensemble mean proportion areas of the seven variables. Inset histograms in (**a–c**) show the frequency (in percent of total area) of time scale distributions, with red colors denoting the time scales of maximum positive correlation between vegetation and drought, blue colors for minimum negative correlation, dark color for significant at $p \leq 0.05$, and light color for non-significant ($p > 0.05$). Inset pie charts indicate the overall proportion of areas of correlation values.

of −0.11 over the region. This indicates an overall drought-tolerant response in springtime, albeit with notable exceptions over the Iberian Peninsula, parts of France, Latvia, Ukraine, and western Russia. The proportion of land area susceptible to drought increased to 45.6% in the month of summer peak growth and 57.8% in the month of autumn senescence (Fig. 1d). The average correlation coefficient for the entire area increased from 0.33 in summer to 0.46 in autumn. The seasonal variations of vegetation correlations to SPEI were consistent among all seven vegetation indicators, with only minor differences among vegetation greenness or structure indicators (NDVI, LAI, and FPAR) and productivity indicators (GPP). The GPP was least affected by drought in the spring and summer months, compared with NDVI, FPAR, and LAI. Three indicators, NIRv, PPI, and SIF, exhibited consistent proportions of areas susceptible to drought (Fig. 1d). The dominant drought time scale differed among seasons, with 5–6 months for the majority area in spring and 2–3 months in summer and autumn (inset histograms in Fig. 1a–c).

The vegetation-drought association was classified into different levels of hierarchical classes, with the two main classes being

humid/subhumid and arid. Humid regions include northern Europe, while subhumid regions can be found in central Europe. Arid regions are typically located in southern Europe, particularly around the Mediterranean and Black Sea (Fig. 2). Figure 2 also demonstrates how the area can be further divided into 5, 8, and 12 sub-classes. These 12 vegetation-drought association classes were further used for evaluating zonal statistics of vegetation-drought responses and to analyze the effects of concurrent hydroclimatic factors.

Sensitivities of vegetation growth to drought and hydroclimatic factors. From the northern humid region to the southern arid region, the sensitivities of vegetation to drought exhibited notable increases, characterized by stronger and more prolonged peak responses (Fig. 3). The average sensitivity during the growing season was around zero in Zone 1–3 (northern Europe, Fig. 2), 0.06 in Zone 4 (mainly Alpine regions), and 0.11 in Zone 5 (Western Russia). The sensitivity values were 0.09–0.20 in Zone 6 and 7 (central European subhumid zones), and 0.19–0.44 in Zone 8–12 (southern European arid zones, Fig. 3). Temporally, the mean sensitivities rose from −0.01 in spring to 0.28 in
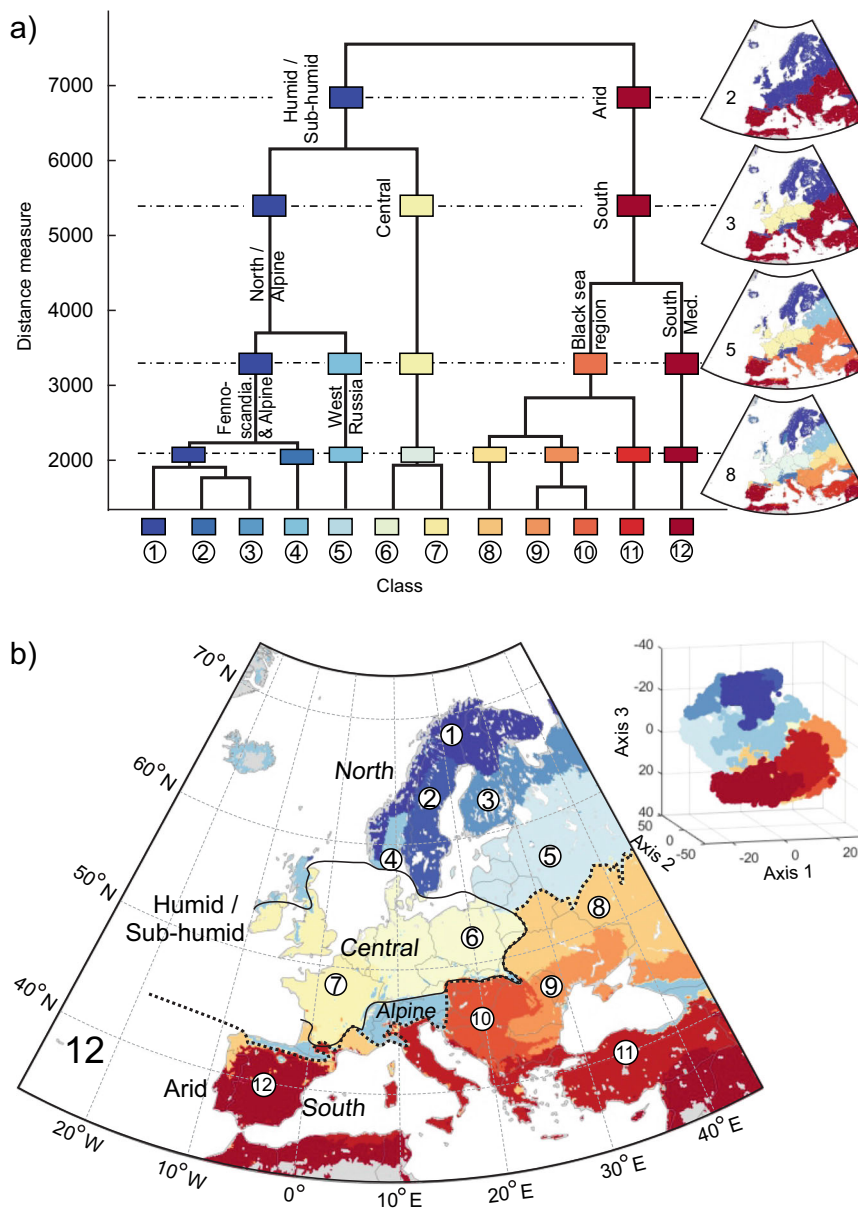
Fig. 2 Hierarchical classification of vegetation-drought association. a The study area may be classified into 2, 3, 5, 8, and 12 different levels of hierarchical classes based on the correlation between the ensemble of vegetation indicators and SPEI from January to December over 1–24 months' time scales. **b** Map of 12 vegetation-drought association classes, with an inset 3-D scatter plot visualizing the separability of these classes using the t-SNE dimension-reduction algorithm.

autumn (Fig. 4a–c). The high response occurred mostly in the month of or within one month before the autumn senescence. In southern Europe, the responses were high throughout the entire growing season. Among the seven vegetation indicators, a higher response in the greenness indicator NDVI was evident during the autumn months. Another two spectral indicators, NIRv and PPI, also showed relatively high responses to SPEI variability. The productivity indicator GPP exhibited a lower response than other vegetation indicators to drought during the summer peak growth months in the central and southern European regions, and the responses to drought of all vegetation indicators converged to a narrow range of high-level during autumn senescence (Fig. 3).

The seven major land cover types from northern to southern Europe all experienced widespread increases in drought sensitivities from spring to autumn (Fig. 4a–c and Fig. 5). The strongest increases occurred in cropland, grassland, and deciduous forests

over central and southern Europe (Fig. 5c, d), which are the predominant land cover types in the area (Fig. 5a). In northern Europe, wetlands exhibited the strongest sensitivities to drought. The evergreen needle leaf forest, the dominant land cover of the region, was found to exhibit lower sensitivity to drought compared to wetlands and shrublands.

During the summer and autumn seasons, vegetation responded more strongly to drought than to other concurrent hydroclimatic factors, evident by the widespread positive drought sensitivities (Fig. 4b, c), i.e., vegetation growth decreased with increasing drought intensity (SPEI decreasing). Along with the role of drought on vegetation growth, other hydroclimatic factors also exerted a range of roles depending on vegetation phenology stages. Vegetation growth decreased with decreasing soil moisture in summer and autumn (positive relations in Fig. 4e, f), with an average sensitivity of 0.12 in both seasons. Vegetation growth overall showed the least response to
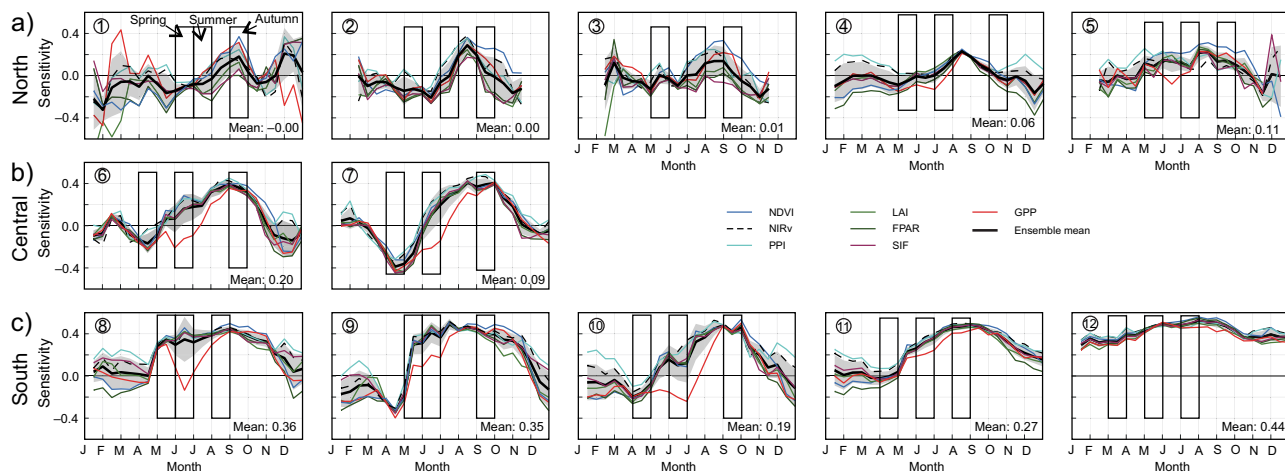
Fig. 3 Annual patterns of vegetation-drought sensitivities. The vegetation-drought sensitivities (γ_d in Eq. 4) over 12 vegetation-drought association zones were determined using ridge regression between a vegetation indicator and hydroclimatic factors including SPEI. **a** North European zones 1–5; **b** central European zones 6–7, and **c** southern European zones 8–12. The shaded area denotes the standard deviation of the ensemble means from the seven vegetation indicators. The numbers denote mean sensitivities in the growing season. The three black rectangles denote the average spring months of growth onset, summer months of peak growth, and autumn months of senescence in each region.

VPD, R_n, and aCO_2 concentration during the summer and autumn seasons (average sensitivities −0.03 to 0.04), except for some local hotspots, for example in middle Sweden the relatively strong positive sensitivity of vegetation growth to autumn VPD (Fig. 4i), and in western Russia, high sensitivity to summer R_n (Fig. 4k). Vegetation responses to hydroclimatic factors in spring differed largely from the other two seasons. On average, drought showed the weakest role in vegetation growth during spring in central Europe (overall sensitivity −0.01, Fig. 4a). The VPD showed strong effects on vegetation growth with an average sensitivity of 0.21 (Fig. 4g), indicating higher spring atmospheric dryness could promote vegetation growth.

Roles of hydroclimatic factors on vegetation-drought sensitivities. Table 1 and Fig. 6 summarize the Spearman correlation coefficients between the sensitivities and hydroclimatic factors aggregated over 12 vegetation-drought association zones during three seasons. The concurrent hydroclimatic factors had varied roles on vegetation-drought sensitivities in different vegetation growth stages. The VPD had the strongest positive significant relationships to the vegetation-drought sensitivities among all the hydroclimatic factors during the entire growing season (Table 1, Fig. 6d–f), with particularly high and significant correlation coefficients in summer and autumn seasons (0.90–0.91, $p \le 0.05$, $n = 12$). The correlation between the vegetation-drought sensitivity and SM over 12 zones was around zero (−0.06 to 0.17, $p > 0.05$, Table 1, Fig. 6a–c), suggesting that the spatial variations of SM had minor roles in vegetation-drought sensitivities. During spring, aCO_2 concentration had weak negative correlations with the vegetation-drought responses (ensemble mean correlation coefficients −0.28, $p > 0.05$, $n = 12$). During autumn, R_n and aCO_2, together with VPD, all had positive significant correlations with vegetation-drought responses, with an ensemble mean correlation coefficient from 0.83 to 0.91 ($p \le 0.05$, $n = 12$, Table 1). The drought sensitives estimated from the seven vegetation indicators exhibited generally consistent correlations to a hydroclimatic factor. A minor inconsistency was found in the roles of aCO_2 and VPD on summer vegetation-drought sensitivities estimated from GPP, which were much weaker compared to estimates from the other six vegetation indicators (Table 1).

Discussion

This study investigates the immediate responses of the multi-faceted nature of vegetation growth to meteorological drought across European biomes. The results show that different satellite-derived vegetation indicators reveal generally consistent patterns of drought responses, which justifies other studies based on a single vegetation indicator from satellites to study drought impacts[32,46,47]. However, we found that the satellite-derived GPP exhibited noticeably weaker responses to drought than the other six indicators during the peak growth (Fig. 3). That the GPP is less affected by drought at the ecosystem level may be explained by resource utilization and re-balancing within the community. Different species adjust resource utilization (niche differentiation), maintaining GPP despite water stress[22]. The optimization of resource usage for maximizing production at the community level may not follow Liebig's law of the minimum for individuals[42,43]. However, it is important to note that vegetation responses to extreme drought events[40] may differ from the results obtained from linear regression analysis. Further research is needed to understand these mechanisms and enhance drought impact assessment.

The association between vegetation and drought varied depending on the month of canopy growth stage. This suggests that droughts can significantly impact ecosystem carbon sequestration due to the high levels of plant photosynthesis and carbon allocation that occur during these periods[51–53]. However, the higher sensitivity of vegetation growth to drought in the summer and autumn seasons compared to spring raises the question of whether larger biomass or productivity contributes to this greater sensitivity. No evidence supports this speculation, as opposite or insignificant relationships were found after further examination between vegetation growth and vegetation-drought sensitivity over the 12 zones. Seasonally varied sensitivity to water stress may be attributed to plant strategies developed during evolution to cope with stressful environments for survival[54–56].

Our findings show that the stronger vegetation responses in central and southern Europe are mainly attributed to the dominant land cover types of the region, such as croplands and grasslands, which can plastically tune their growth to water availability, a physiological strategy after long-term natural adaptation or human selection during farming practice to fit subhumid and arid climates[57]. However, in northern humid
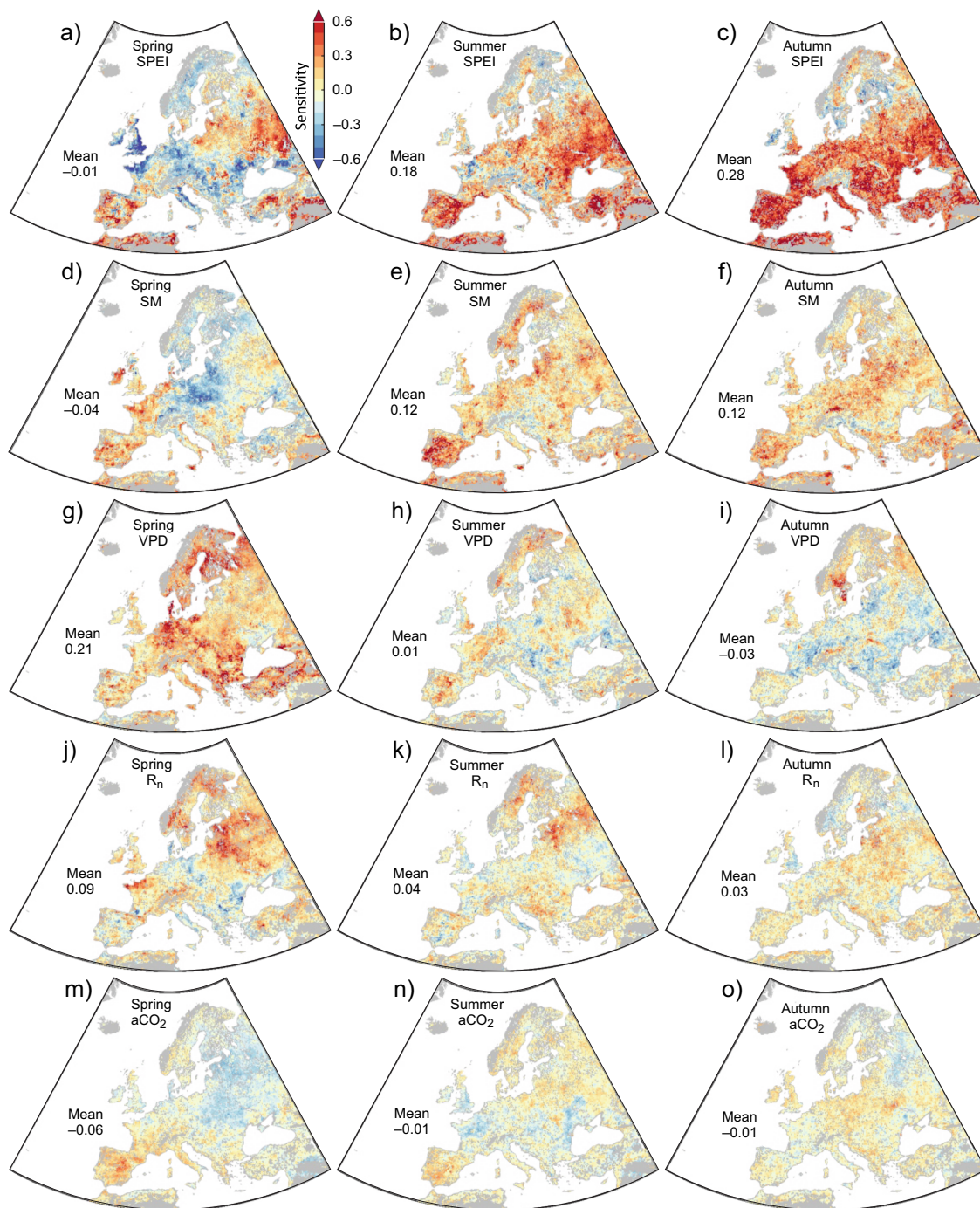
Fig. 4 Map of vegetation sensitivities to drought and four concurrent hydroclimatic factors. a–c Vegetation sensitivities to drought, γ_d using SPEI.
d–f Vegetation sensitivities to SM——soil moisture, **g–i** vegetation sensitivities to VPD——vapor pressure deficit, **j–l** vegetation sensitivities to R_n——net
radiation, and **m–o** vegetation sensitivities to aCO$_2$——atmospheric CO_2 concentration, during three vegetation seasons. These maps show the ensemble
mean sensitivities using seven vegetation indicators at the time scale when vegetation-drought correlation reaches the strongest level among time scales
ranging from 1 to 24 months. Positive values indicate vegetation growth increasing with increases in hydroclimatic factors (or decreases in drought
intensity), and negative values indicate the opposite.

regions, wetlands had a stronger drought sensitivity than other
land cover types, making them more vulnerable to increasing
drought with changing climate[58]. We used dimension-reduction
and hierarchical classification techniques to produce a map of the
association between vegetation and drought in Europe. The map
shows a resemblance to the Köppen-Geiger climate classification
map, which characterizes empirical fundamental biome dis-
tributions based on monthly climate factors[59–61]. By taking into

account the drought effects (combining precipitation and energy)
on monthly vegetation growth, our mapping approach has the
potential to provide a realized vegetation distribution under
vegetation-climate interactions. Vegetation distribution study
using climatic water balance has been shown to be more reliable
than temperature and precipitation-based approaches[62].
We revealed seasonal shifts in hydroclimatic constraints on
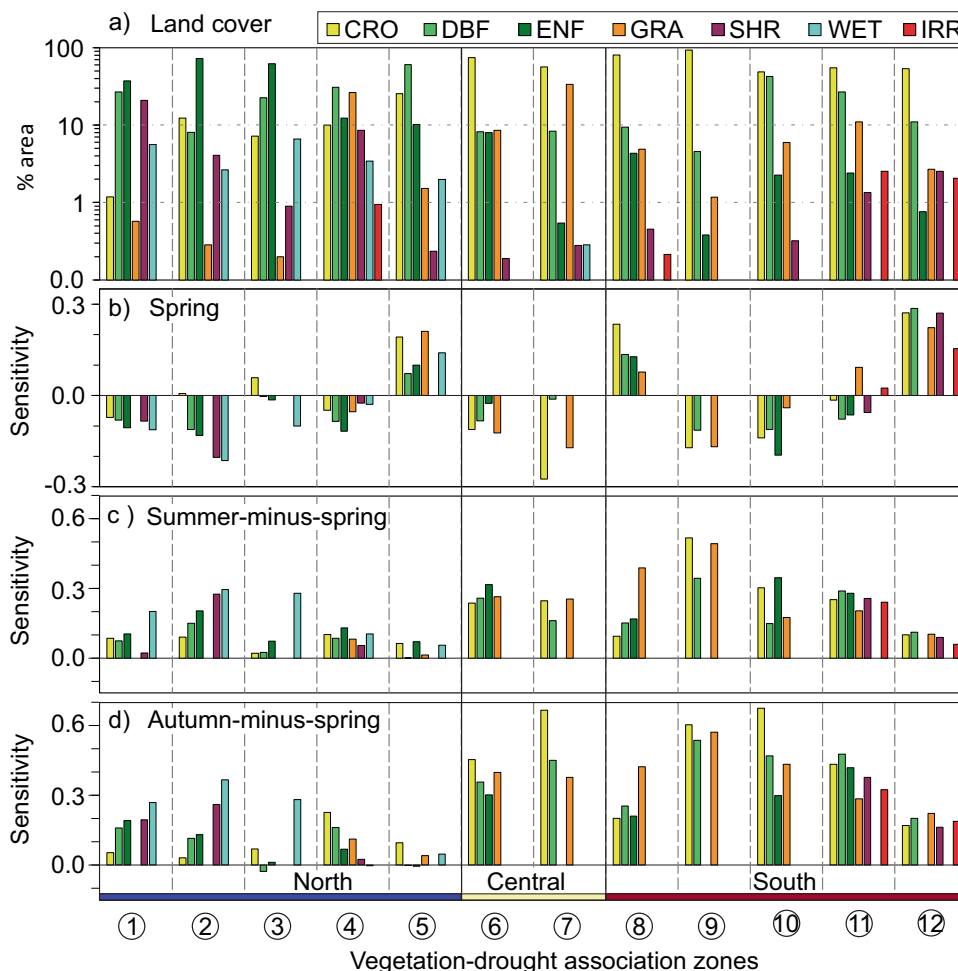vegetation growth and vegetation sensitivities to drought,

Fig. 5 Statistics of seven aggregated land covers in 12 vegetation-drought association zones. a Proportion of areas, **b** drought sensitivities in spring, **c** difference of drought sensitivities in summer against spring, and **d** difference of drought sensitivities in autumn against spring. CRO——non-irrigated cropland, DBF——deciduous broadleaf and mixed forest, ENF——evergreen needle leaf forest, GRA——grassland, SHR——shrubland, WET——wetland, IRR——irrigated cropland. Note that the sensitivities for landcover proportion less than 1% of the association zone are omitted due to the small number of pixels.

Table 1 Spearman correlation coefficients of the vegetation-drought sensitivities to concurrent hydroclimatic factors.

Season	Environmental variable	Vegetation spectral indicators			Vegetation biophysical indicators				Ensemble mean
		NDVI	NIRv	PPI	FPAR	LAI	SIF	GPP	
Spring months of growth onset	SM	−0.08	−0.06	0.00	−0.08	−0.09	−0.07	−0.06	−0.06
	VPD	0.50	0.57	0.55	0.45	0.46	0.58	0.36	0.45
	Rn	0.27	0.24	0.29	0.23	0.22	0.22	0.22	0.27
	aCO_2	−0.14	−0.21	−0.34	−0.29	−0.34	−0.34	−0.26	−0.28
Summer months of peak growth	SM	0.07	−0.03	0.01	0.03	0.04	−0.06	−0.13	0.02
	VPD	**0.87**	**0.78**	**0.78**	**0.88**	**0.92**	**0.80**	0.51	**0.90**
	Rn	0.10	−0.08	−0.02	0.19	0.18	−0.04	0.06	0.08
	aCO_2	0.38	0.66	0.62	0.51	0.50	**0.69**	−0.02	0.49
Autumn months of growth senescence	SM	0.08	0.09	0.10	0.08	0.15	0.15	0.00	0.17
	VPD	**0.85**	**0.94**	**0.96**	**0.90**	**0.90**	**0.95**	**0.89**	**0.91**
	Rn	**0.78**	**0.89**	**0.92**	**0.87**	**0.89**	**0.94**	**0.78**	**0.89**
	aCO_2	**0.74**	**0.82**	**0.85**	**0.77**	**0.78**	**0.87**	**0.72**	**0.83**

The correlation coefficients are estimated from aggregated statistics over 12 vegetation-drought association zones and three phenological seasons in Fig. 6. The **bold** fonts indicate significant correlations at $p \le 0.05$.

consistent with the intra-annual shifts in another study[17]. The transient atmospheric dryness indicator VPD and the energy indicator Rn played strong roles in vegetation growth in spring, whereas SM played a strong role in summer and autumn[53,63].

Spatially, the zonal aggregated feature exhibited that VPD had the greatest role in the vegetation responses to drought, with higher VPD leading to stronger drought responses in summer and autumn (Fig. 6e, f). Surprisingly, the soil moisture effects on the
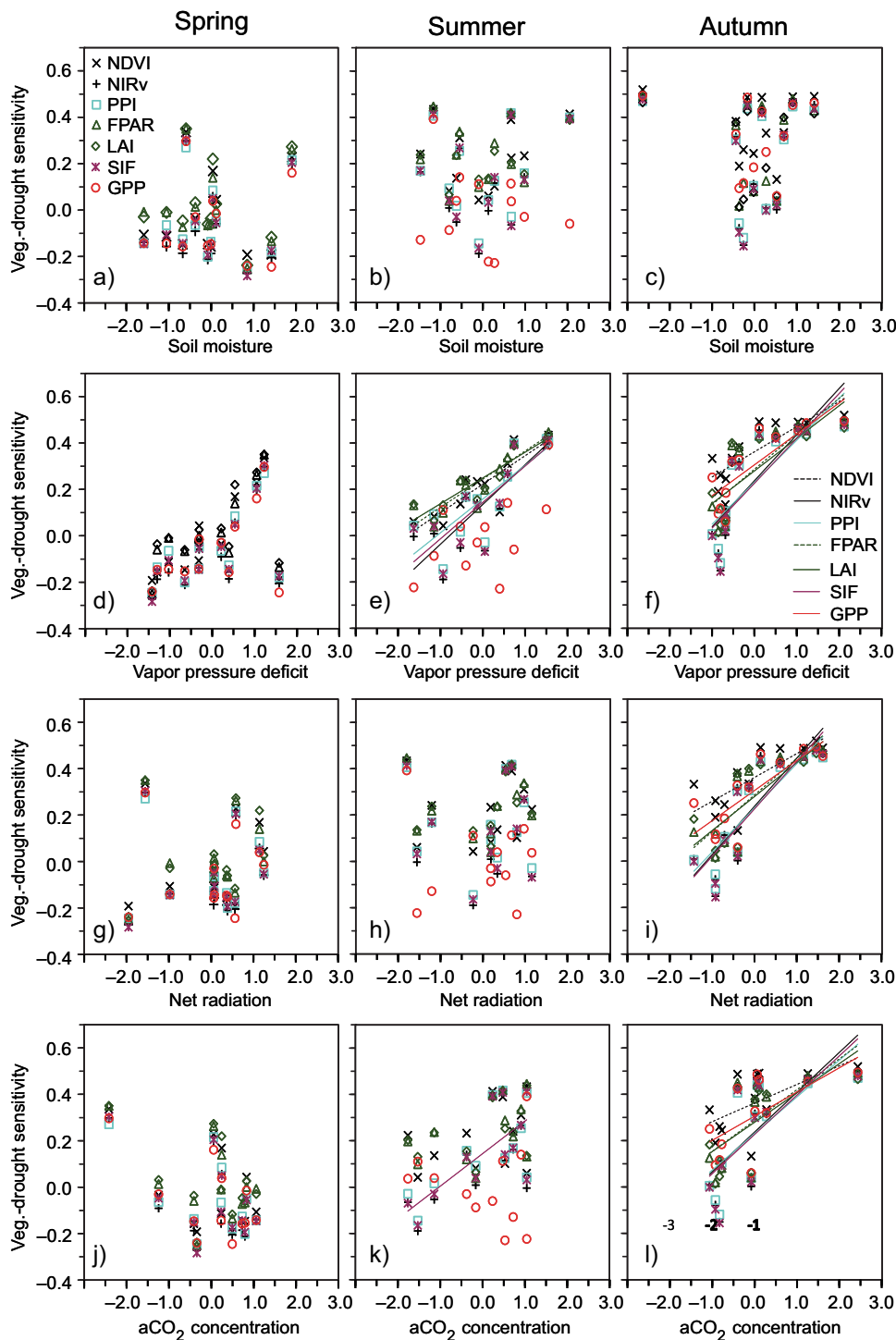
Fig. 6 Spatial relationships between vegetation-drought sensitivity and hydroclimatic factors. a–c The relationship between vegetation-drought sensitivity (γ_d) and soil moisture, **d–f** the relationship between γ_d and vapor pressure deficit, **g–i** the relationship between γ_d and net radiation, **j–l** the relationship between γ_d and aCO$_2$ concentration during three vegetation seasons. The four hydroclimatic factors are arranged in rows for three vegetation seasons (arranged in columns). The linear fitting lines indicate that the relationships are significant at $p \leq 0.05$ (Spearman correlation in Table 1). The hydroclimatic factors are standardized by the mean and standard deviation in each season so that the slopes of linear fitting lines are comparable across different factors and seasons.

sensitivity of vegetation to meteorological drought were weak (Fig. 6, Table 1), even though soil moisture did influence vegetation growth (Fig. 3). We may conclude that seasonal variations in SM contributed to seasonal variations of vegetation growth (Fig. 4d–f), and spatial variations in SM had no observable effects on vegetation sensitivity to meteorological drought (Fig. 6a–c).

The spatial variation of VPD, instead, played an important role in the variations of vegetation sensitivities to drought. Therefore, spatial increases in vegetation sensitivity to drought were attributed to VPD increase and seasonal increases in vegetation sensitivities to drought can be further exacerbated by SM scarcity[17,20,63]. This suggests that a lack of SM can impede

vegetation productivity, but it is the high VPD that consistently increases vegetation's vulnerability to drought[64].

Vegetation sensitivities to drought across global drylands were found to have increased during the past four decades, and the increase was attributed to the elevated aCO_2[22]. Our results revealed divergent sub-seasonal perspectives. European dry regions were more sensitive to drought than humid regions, and the higher aCO_2 in dry regions could significantly increase vegetation susceptibility to drought in the autumn season (Fig. 6l), with no effects in spring (Fig. 6j). A plant-centric view is that elevated aCO_2 could mitigate drought impacts on vegetation[19] because plants can use water efficiently during photosynthesis with high aCO_2. However, the enhanced photosynthesis from elevated aCO_2 could also lead to water depletion due to excessive consumption by CO_2-boosted plant growth, particularly in areas where water is already scarce[22,65]. In summary, the effect of elevated aCO_2 on vegetation-drought sensitivity is still a matter of debate[66]. The outcome depends on various factors such as plant species, growing stage, water and nutrient availability, and the intensity of the drought event. The situation can be further complicated by legacy effects since the saved evaporative water loss from elevated aCO_2 allows more partitioning of precipitation into runoff and soil water for later use in another area.

Conclusions

We found that the sensitivity of vegetation to meteorological drought is higher in autumn than in spring, indicating a greater susceptibility of vegetation growth to drought in autumn compared to spring. Therefore, it is crucial to prioritize water management strategies during the late growing season to enhance primary production, carbon sequestration, and crop yield, taking into account the anticipated European climate change scenario of wet springs and dry summers.

Vegetation in southern regions demonstrates higher sensitivity to drought than in the northern regions. The spatial pattern of the association between vegetation and drought resembles the climate zone of the distribution of vegetation. Different land cover types also exhibit varying sensitivities to drought. Cropland, grassland, and deciduous forests in central and southern Europe show the strongest sensitivities to drought. Wetlands in northern Europe are also highly sensitive to drought, whereas evergreen needle leaf forests exhibit lower sensitivity compared to other land cover types. This study utilized a hierarchical classification to categorize the vegetation-drought association into different classes, facilitating the understanding of regional variations in vegetation response to drought.

The study also identified varying roles of concurrent hydroclimatic factors on vegetation growth and vegetation-drought sensitivities. In northern Europe, wet soil and low VPD tend to inhibit springtime vegetation growth. SM primarily affects vegetation growth in summer and autumn, whereas it has weak role in vegetation sensitivity to meteorological drought. In areas with high VPD, vegetation demonstrates strong responses to drought throughout the year, particularly during summer and autumn. Although aCO_2 plays a minor role in the interannual variability of vegetation growth, vegetation in high aCO_2 regions exhibits considerably high sensitivity to autumn drought but weak sensitivity to spring drought. The seven vegetation indicators used to estimate drought sensitivities generally exhibit similar seasonal patterns and consistent correlations with hydroclimatic factors. However, it is worth noting that the GPP-derived drought sensitivity appears weaker and shows less influence from summer VPD and aCO2 compared to the other vegetation indicators.

Our research provides insights into the immediate effects of meteorological drought on vegetation across Europe over space and time. The findings contribute to a better understanding of vegetation responses to drought and help elucidate the effects of soil moisture, vapor pressure deficit, radiative energy, and atmospheric CO_2 on vegetation development during drought stress.

Methods

Study area. We focus on European biomes across a climate gradient from northern cold humid tundra to southern hot arid desert, covering latitudes 33°N to 74°N and longitudes 27°W to 45°E. Vegetated land cover was aggregated into seven major types: non-irrigated cropland (CRO), irrigated cropland (IRR), grassland (GRA), deciduous broadleaf/mixed forest (DBF), evergreen needleleaf forest (ENF), shrubland (SHR), and wetland (WET), based on Corine Land Cover (CLC) 2018 (Version 2020_20u1). The European Space Agency (ESA) Climate Change Initiative (CCI) land cover product was used for regions outside the CLC coverage (ESA 2017). Both landcover datasets show good agreement, justifying their merging[67]. Pixels that changed land cover type from 2000 to 2020 were identified in the CCI product and excluded from this study. The study area (Fig. 7a) is dominated by non-irrigated cropland (40.7%), followed by broadleaf and mixed forests (22.3%), needleleaf forest (11.7%), and grassland (7.8%). The study area, in general, has dry climate conditions in the south, subhumid in the center, and humid in the northern part and in the alpine mountains (Fig. 7b).

Climate data. Daily precipitation data were collected from the Multi-Source Weighted-Ensemble Precipitation dataset (MSWEP http://www.gloh2o.org/mswep/). MSWEP provides global precipitation estimates (P) by optimally merging rain gauge, satellite, and reanalysis data at 0.1-degree resolution from 1979 to the present[68]. The daily atmospheric demand (AED, or potential evapotranspiration) data were collected from Bristol's potential evapotranspiration dataset at 0.1-degree resolution for the global land surface from 1981 to 2020 (https://data.bris.ac.uk/data/). The AED data are calculated using FAO's Penman-Monteith formulation[69] with climate variables from ERA5-Land[70]. The P and AED were used to calculate SPEI in this study (Section 2.4).

We also collected monthly SM (0–100 cm), VPD, and R_n data from the Global Land Data Assimilation System (GLDAS) Noah Land Surface Model L4 monthly 0.25×0.25 degree V2.1 dataset GLDAS_NOAH025_M[71], to investigate the independent roles of these hydroclimatic factors on vegetation growth and vegetation-drought responses. We utilized the water component (SM) and energy components (R_n, VPD) from the same land surface model to consider their coupling nature[72]. We collected aCO_2 column-mean molar fraction from Copernicus Atmosphere Monitoring Service (CAMS) global greenhouse gas reanalysis monthly averaged fields dataset to investigate the role of aCO_2 in vegetation-drought responses. All these data (Table 2) were resampled to 0.1-degree resolution and half-month step using bilinear spatial interpolation and linear temporal interpolation, consistent with the drought indices.

Remotely sensed vegetation data. Assessing drought response on vegetation growth at local, regional, and global scales can be done using remotely sensed indicators. Vegetation growth has different facets[15]; therefore, drought impacts on vegetation growth have also multiple aspects. We used an ensemble of indicators for vegetation growth and productivity derived from different satellite platforms to examine vegetation responses to drought (Table 2). The NDVI is one of the most widely used greenness
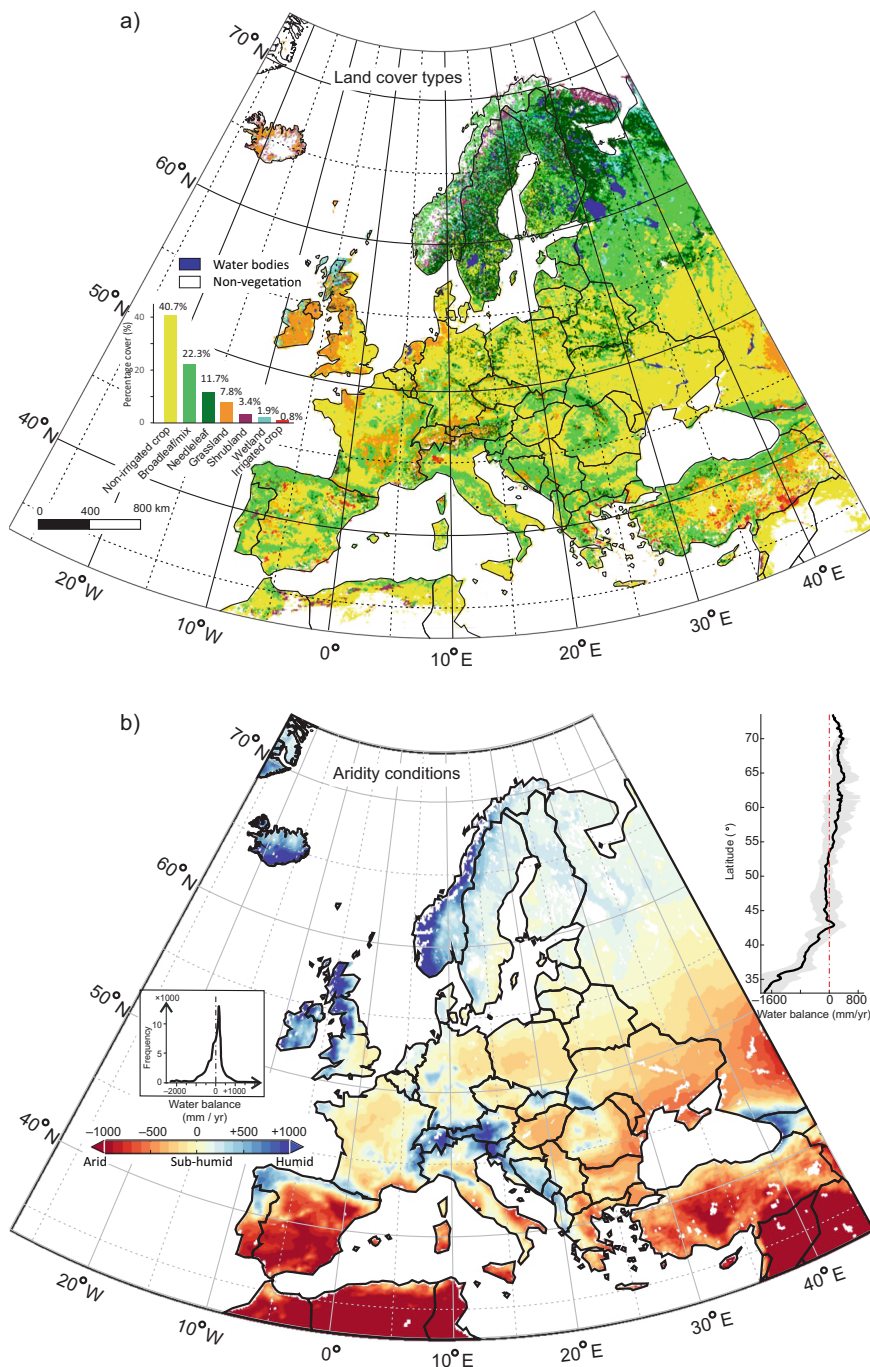
Fig. 7 Maps of land cover and aridity conditions of the study area. a Vegetated land cover types and **b** climatic aridity conditions of the study area. Vegetated land covers are aggregated into seven major classes based on the Corine Land Cover (CLC) 2018 and the ESA CCI land cover product 2020, with inset bar chart showing the legend and the percentage cover of the seven classes. Climatic aridity conditions are indicated by the mean annual water balance (P-AED) during 2000–2020, with insets showing distribution frequencies and latitudinal profile.

indices for studying vegetation growth and environmental impact[73]. The near-infrared reflectance of vegetation NIRv[74], is another indicator that strongly correlates to leaf chlorophyll photon interception during photosynthesis processes. The plant phenology index (PPI)[75] is a physically based vegetation index for photosynthetically active leaf area quantity and has good relation with vegetation productivity. Furthermore, several vegetation biophysical variables derived from satellite observations, such as Leaf Area Index (LAI), FPAR, solar-induced fluorescence (SIF), and gross primary productivity (GPP) estimations, can be used to investigate drought impacts on vegetation[16,40,46,76].

Three of the aforementioned vegetation indicators, NDVI, NIRv, and PPI, were calculated using the Moderate Resolution Imaging Spectroradiometer (MODIS) nadir bi-directional reflectance distribution function (BRDF) adjusted reflectance (NBAR) product (Version 6.0) at a daily time step and 0.05-degree spatial resolution:

$$NDVI = \frac{DVI}{NIR + Red} \qquad (1)$$

$$NIRv = NDVI \times NIR \qquad (2)$$

Table 2 Summary of the data used in this study.

Variables	Dataset/sensors	Temporal resolution	Spatial resolution	Source
Climate and environmental variables				
Precipitation	MSWEP	Daily	0.1° × 0.1°	http://www.gloh2o.org/mswep/
PET	Bristol PET	Daily	0.1° × 0.1°	https://data.bris.ac.uk/data/dataset/qb8ujazzda0s2aykkv0oq0ctp
Soil moisture, VPD, Net radiation	GLDAS	Monthly	0.25° × 0.25°	https://disc.gsfc.nasa.gov/datasets/GLDAS_NOAH025_M_2.1/summary?keywords=NOAH025
aCO$_2$ concentration	CAMS	Monthly	0.75° × 0.75°	https://ads.atmosphere.copernicus.eu/cdsapp#!/dataset/cams-global-ghg-reanalysis-egg4-monthly
Vegetation indicators				
NDVI, NIRv, PPI	MODIS	daily	0.05° × 0.05°	https://lpdaac.usgs.gov/products/mcd43c4v006/
FPAR, LAI	SPOT/VGT, PROBA-V, Sentinel-3	10-day	1 km × 1 km and 1/3 km × 1/3 km	https://land.copernicus.eu/global/products/lai https://land.copernicus.eu/global/products/fapar
SIF	OCO-2, MODIS	Monthly	0.05° × 0.05°	https://osf.io/8xqy6/ https://daac.ornl.gov/VEGETATION/guides/FluxSat_GPP_FPAR.html
GPP	FluxSat	Daily	0.05° × 0.05°	
Land cover types				
LC	CLC	–	100 m	https://sdi.eea.europa.eu/catalogue/static/api/records/93eede6e-c196-40e3-9253-7f2237b49de1
	CCI-LC	Yearly	300 m	https://www.esa-landcover-cci.org/?q=node/164

$$PPI = -K \times \ln\left(\frac{M - DVI}{DVI - 0.09}\right) \quad (3)$$

where $DVI = NIR - Red$, the difference vegetation index between Red and near-infrared reflectance (NIR). M is the maximum DVI of each pixel during 2000−2020, and K is a factor calculated from M, the solar zenith angle, and the diffuse fraction of radiation. Four biophysical vegetation indicators, LAI, FPAR, SIF, and GPP, were directly downloaded from open sources. The LAI and FPAR are generated from three satellite platforms: SPOT/VGT, PROBA-V, and Sentinel-3, available from the Copernicus Global Land Service (CGLS, https://land.copernicus.eu/global/ themes/vegetation). The clear sky daily SIF data were from the contiguous solar-induced fluorescence (CSIF) dataset[77], and GPP from the Global MODIS and FLUXNET-derived Daily Gross Primary Production, V2 FluxSat 2.0[78]. Both SIF and GPP datasets are generated using neural network-based models trained by MODIS NBAR reflectance data. Specifically, CSIF is from the downscaling of coarse resolution Orbiting Carbon Observatory-2 observations and FluxSat GPP from the upscaling of tower-based measurements in the global FLUXNET 2015 networks (Joiner and Yoshida 2020).

All seven vegetation indicators were aggregated to 0.1-degree resolution at a half-month step to investigate vegetation-drought associations and responses. To investigate sub-seasonal vegetation responses to drought, we estimated vegetation phenology, including the start of the growing season, the peak of the growing season, and the end of the growing season, from the PPI time series using the TIMESAT software[79], following ref. [80]. To facilitate comparison, we particularly summarize the results for three distinct months of a year: the month of spring onset of vegetation growth, the month of summer peak growth, and the month of autumn senescence.

Calculation of SPEI. The SPEI was calculated for time scales from 1 to 24 months at a half-month step. First, the accumulated water balance D was calculated as:

$$D_n^k = \sum_{i=0}^{2n-1} \left(P_{k-i} - AED_{k-i} \right) \quad (4)$$

where k is the time position at a half-month step, and n is the time scale ($n = 1, 2, …, 24$ months). Second, D was transformed to normal distribution $N(0, 1)$ using a 3-parameter log-logistic distribution to obtain SPEI for each half-month-of-year and each time scale over a reference period of 1981–2020 using the script at https://digital.csic.es/handle/10261/10002 following Vicente-Serrano et al.[23].

Data analysis. The impact of SPEI interannual variability on vegetation growth was evaluated by examining the correlation between vegetation indicators and SPEI, following a similar approach as in Vicente-Serrano et al.[32]. Specifically, we calculated the simple Spearman correlation between a vegetation indicator and SPEI for each half-month from January to December, covering the period from 2000 to 2020 with 24 time series for each pixel. The computation was performed for seven vegetation indicators and 24 time scales. The Spearman rank correlation rather than Pearson linear correlation was used to account for the potential nonlinear nature of vegetation response to water availability. Furthermore, the first differencing variables were employed instead of raw data to account for non-stationary time series and potential spurious correlation[81]. Each pixel yielded 4032 correlation coefficients (24 × 7 × 24). These correlation coefficients were then used in two tasks: (1) To classify spatial patterns of the vegetation-drought association for the 1.2×10^5

vegetated land pixels in total. (2) To determine the dominant drought time scale, at which of 1 to 24 months' time scale the correlation between the vegetation indicator and SPEI was strongest in each half-month of a year.

In the first task, we used the *t*-distributed stochastic neighbor embedding method t-SNE[82] to reduce the 4032 dimensions to 3-D. Based on Euclidian distance measures of the 3-D data, the entire region was then classified into different vegetation-drought association zones using a hierarchical classification method. A fixed seed is specified before the tSNE processing to allow for repeatability in the unsupervised classification. The number of classes in a hierarchical classification system was chosen from separable distance measures to avoid merging sub-classes at different hierarchical levels.

In the second task, the correlation at the dominant time scale could be either negative or positive, depending on its absolute value. A positive value indicates that vegetation growth is sensitive to drought, and the drought has a prohibition effect on vegetation growth at the dominant time scale. A negative correlation indicates vegetation growth is contrarily promoted by the metrological drought condition. The vegetation-drought sensitivity was estimated in the following analysis for the SPEI at the dominant time scales.

A linear model was used to estimate the sensitivities of vegetation growth to meteorological drought. To separate the unique contribution of meteorological drought from other concurrent hydroclimatic factors on vegetation growth, we included SM, VPD, R_n, and aCO_2 in the multiple linear regression:

$$y = \alpha + \gamma_d SPEI + \sum_{i=1}^{4} \gamma_i \cdot x_i + \beta t + \varepsilon \qquad (5)$$

where y is a vegetation indicator (NDVI, NIRv, PPI, LAI, FPAR, SIF, or GPP), γ_d is the vegetation sensitivity to drought. γ_i (i = 1,2,..., 4) is the vegetation sensitivities to the four concurrent hydroclimatic factors, SM, VPD, R_n, and aCO_2. The regressor *t* is an augment term to address potential spurious regression caused by trends in variables, which is preferred over the explicit detrending method to address stochastic trends[83].

Equation (5) was transformed to the first difference form to eliminate the constant α. The five sensitivity parameters (regression coefficients γ_d and γ_1 to γ_4) were estimated using ridge regression by standardizing regressors (the first differences of *SPEI*, SM, VPD, R_n, and aCO_2, respectively). The regression coefficients reflect the changes in response variables corresponding to unit changes in the standardized regressors. They are unitless and comparable across models and predictors. The ridge regression reduced the variability of regression slopes, which is particularly useful in the case of multicollinearity among hydroclimatic factors. No significant level is reported for slopes estimated from ridge regression since the variance of slopes is manipulatively suppressed by a ridge factor. The ridge factor was chosen following ref. [84] using the script at https://se.mathworks.com/matlabcentral/fileexchange/121008-autoridge. All the analyses were implemented using MATLAB (R2022a) Statistics and Machine Learning Toolbox™ on a high-performance computing (HPC) system of the Swedish National Infrastructure for Computing (SNIC).

Data availability
All the original data resources are publicly accessible and listed in Table 2. The datasets generated in this study are available in the Figshare repository, https://doi.org/10.6084/m9.figshare.23653110.

Code availability
All analyses were implemented using MATLAB (R2022a) Statistics and Machine Learning Toolbox. Scripts for SPEI calculation are from script at https://digital.csic.es/

handle/10261/10002. TIMESAT for phenology processing is freely available at https://web.nateko.lu.se/timesat/timesat.asp?cat=6. Automatic ridge regression is from https://se.mathworks.com/matlabcentral/fileexchange/121008-autoridge.

References
1. Wilhite, D. A. & Glantz, M. H. Understanding the drought phenomenon: the role of definitions. *Water Int.* **10**, 111–120 (1985).
2. Vicente-Serrano, S. M. et al. Global drought trends and future projections. *Philos. Trans. R. Soc. A Math. Phys. Eng. Sci.* **380**, 20210285 (2022).
3. Seneviratne, S. I. et al. *Climate Change 2021: The Physical Science Basis. Contribution of Working Group I to the Sixth Assessment Report of the Intergovernmental Panel on Climate Change* (eds Masson-Delmotte, V. et al.) 1513–1766 (Cambridge University Press, 2021).
4. Allen, C. D., Breshears, D. D. & McDowell, N. G. On underestimation of global vulnerability to tree mortality and forest die-off from hotter drought in the Anthropocene. *Ecosphere* **6**, art129 (2015).
5. Vicente-Serrano, S. M., Quiring, S. M., Peña-Gallardo, M., Yuan, S. & Domínguez-Castro, F. A review of environmental droughts: increased risk under global warming? *Earth Sci. Rev.* **201**, 102953 (2020).
6. Ciais, P. et al. Europe-wide reduction in primary productivity caused by the heat and drought in 2003. *Nature* **437**, 529 (2005).
7. Pellizzari, E. et al. Diverging shrub and tree growth from the Polar to the Mediterranean biomes across the European continent. *Glob. Change Biol.* **23**, 3169–3180 (2017).
8. Koelemeijer, I. A. et al. Interactive effects of drought and edge exposure on old-growth forest understory species. *Landsc. Ecol.* **37**, 1839–1853 (2022).
9. Tilman, D. & El Haddi, A. Drought and biodiversity in Grasslands. *Oecologia* **89**, 257–264 (1992).
10. Büntgen, U. et al. Recent European drought extremes beyond Common Era background variability. *Nat. Geosci.* **14**, 190–196 (2021).
11. Conradt, T. et al. Cross-sectoral impacts of the 2018–2019 Central European drought and climate resilience in the German part of the Elbe River basin. *Reg. Environ. Change* **23**, 32 (2023).
12. García-Herrera, R. et al. The European 2016/17 drought. *J. Clim.* **32**, 3169–3187 (2019).
13. Cammalleri, C. et al. *Global Warming and Drought Impacts in the EU* (Publications Office of the European Union, 2020).
14. Naumann, G., Cammalleri, C., Mentaschi, L. & Feyen, L. Increased economic drought impacts in Europe with anthropogenic warming. *Nat. Clim. Change* **11**, 485–491 (2021).
15. Hilty, J., Muller, B., Pantin, F. & Leuzinger, S. Plant growth: the what, the how, and the why. *N. Phytol.* **232**, 25–41 (2021).
16. Deng, Y. et al. Divergent seasonal responses of carbon fluxes to extreme droughts over China. *Agric. For. Meteorol.* **328**, 109253 (2023).
17. Denissen, J. M. C. et al. Widespread shift from ecosystem energy to water limitation with climate change. *Nat. Clim. Change* **12**, 677–684 (2022).
18. Stocker, B. D. et al. Drought impacts on terrestrial primary production underestimated by satellite monitoring. *Nat. Geosci.* **12**, 264–270 (2019).
19. Swann, A. L. S., Hoffman, F. M., Koven, C. D. & Randerson, J. T. Plant responses to increasing CO_2 reduce estimates of climate impacts on drought severity. *Proc. Natl Acad. Sci. USA* **113**, 10019–10024 (2016).
20. Liu, L. et al. Soil moisture dominates dryness stress on ecosystem production globally. *Nat. Commun.* **11**, 4892 (2020).
21. Vicente-Serrano, S. M. et al. The uncertain role of rising atmospheric CO_2 on global plant transpiration. *Earth Sci. Rev.* **230**, 104055 (2022).
22. Zhang, Y. et al. Increasing sensitivity of dryland vegetation greenness to precipitation due to rising atmospheric CO_2. *Nat. Commun.* **13**, 4875 (2022).
23. Vicente-Serrano, S. M., Beguería, S. & López-Moreno, J. I. A multiscalar drought index sensitive to global warming: the standardized precipitation evapotranspiration index. *J. Clim.* **23**, 1696–1718 (2010).
24. Dracup, J. A., Lee, K. S. & Paulson, E. G. Jr. On the definition of droughts. *Water Resour. Res.* **16**, 297–302 (1980).
25. Dai, A., Zhao, T. & Chen, J. Climate change and drought: a precipitation and evaporation perspective. *Curr. Clim. Change Rep.* **4**, 301–312 (2018).
26. Peña-Gallardo, M. et al. Complex influences of meteorological drought time-scales on hydrological droughts in natural basins of the contiguous Unites States. *J. Hydrol.* **568**, 611–625 (2019).
27. Vicente-Serrano, S. M. et al. Evidence of increasing drought severity caused by temperature rise in southern Europe. *Environ. Res. Lett.* **9**, 044001 (2014).
28. Vicente-Serrano, S. M., McVicar, T. R., Miralles, D. G., Yang, Y. & Tomas-Burguera, M. Unraveling the influence of atmospheric evaporative demand on

drought and its response to climate change. *WIREs Clim. Change* **11**, e632 (2020).

29. Bachmair, S., Tanguy, M., Hannaford, J. & Stahl, K. How well do meteorological indicators represent agricultural and forest drought across Europe? *Environ. Res. Lett.* **13**, 034042 (2018).

30. Tian, L., Yuan, S. & Quiring, S. M. Evaluation of six indices for monitoring agricultural drought in the south-central United States. *Agric. For. Meteorol.* **249**, 107–119 (2018).

31. Wang, H. et al. Monitoring winter wheat drought threat in Northern China using multiple climate-based drought indices and soil moisture during 2000–2013. *Agric. For. Meteorol.* **228–229**, 1–12 (2016).

32. Vicente-Serrano, S. M. et al. Response of vegetation to drought time-scales across global land biomes. *Proc. Natl Acad. Sci. USA* **110**, 52–57 (2013).

33. Gouveia, C. M., Trigo, R. M., Beguería, S. & Vicente-Serrano, S. M. Drought impacts on vegetation activity in the Mediterranean region: an assessment using remote sensing data and multi-scale drought indicators. *Glob. Planet. Change* **151**, 15–27 (2017).

34. Spinoni, J., Naumann, G. & Vogt, J. V. Pan-European seasonal trends and recent changes of drought frequency and severity. *Glob. Planet. Change* **148**, 113–130 (2017).

35. Spinoni, J., Vogt, J. V., Naumann, G., Barbosa, P. & Dosio, A. Will drought events become more frequent and severe in Europe? *Int. J. Climatol.* **38**, 1718–1736 (2018).

36. van Kampen, R., Fisichelli, N., Zhang, Y.-J. & Wason, J. Drought timing and species growth phenology determine intra-annual recovery of tree height and diameter growth. *AoB PLANTS* **14**, plac012 (2022).

37. Li, M., Ge, C., Zong, S. & Wang, G. Drought assessment on vegetation in the Loess Plateau using a phenology-based vegetation condition index. *Remote Sens.* **14**, 3043 (2022).

38. Wu, M. et al. Drought legacy in sub-seasonal vegetation state and sensitivity to climate over the Northern Hemisphere. *Geophys. Res. Lett.* **49**, e2022GL098700 (2022).

39. Wu, C. et al. Increased drought effects on the phenology of autumn leaf senescence. *Nat. Clim. Change* **12**, 943–949 (2022).

40. Mohammadi, K., Jiang, Y. & Wang, G. Flash drought early warning based on the trajectory of solar-induced chlorophyll fluorescence. *Proc. Natl Acad. Sci. USA* **119**, e2202767119 (2022).

41. Sun, Y., Wang, C., Chen, H. Y. H. & Ruan, H. Response of plants to water stress: a meta-analysis. *Front. Plant Sci.* **11** https://doi.org/10.3389/fpls.2020.00978 (2020).

42. Danger, M., Daufresne, T., Lucas, F., Pissard, S. & Lacroix, G. Does Liebig's law of the minimum scale up from species to communities? *Oikos* **117**, 1741–1751 (2008).

43. Tang, J. & Riley, W. J. Finding Liebig's law of the minimum. *Ecol. Appl.* **31**, e02458 (2021).

44. Körner, C. Paradigm shift in plant growth control. *Curr. Opin. Plant Biol.* **25**, 107–114 (2015).

45. Samaniego, L. et al. Anthropogenic warming exacerbates European soil moisture droughts. *Nat. Clim. Change* **8**, 421–426 (2018).

46. Ivits, E., Horion, S., Erhard, M. & Fensholt, R. Assessing European ecosystem stability to drought in the vegetation growing season. *Glob. Ecol. Biogeogr.* **25**, 1131–1143 (2016).

47. Ivits, E., Horion, S., Fensholt, R. & Cherlet, M. Drought footprint on European ecosystems between 1999 and 2010 assessed by remotely sensed vegetation phenology and productivity. *Glob. Change Biol.* **20**, 581–593 (2014).

48. He, W. et al. *Proc. IGARSS 2019—2019 IEEE International Geoscience and Remote Sensing Symposium*, 9273–9276 (2019).

49. Hong, S. et al. Contrasting temperature effects on the velocity of early- versus late-stage vegetation green-up in the Northern Hemisphere. *Glob. Change Biol.* **28**, 6961–6972 (2022).

50. Jin, H., Jönsson, A. M., Bolmgren, K., Langvall, O. & Eklundh, L. Disentangling remotely-sensed plant phenology and snow seasonality at northern Europe using MODIS and the plant phenology index. *Remote Sens. Environ.* **198**, 203–212 (2017).

51. Krejza, J. et al. Disentangling carbon uptake and allocation in the stems of a spruce forest. *Environ. Exp. Bot.* **196**, 104787 (2022).

52. Salomón, R. L. et al. The 2018 European heatwave led to stem dehydration but not to consistent growth reductions in forests. *Nat. Commun.* **13**, 28 (2022).

53. Zhang, Y., Parazoo, N. C., Williams, A. P., Zhou, S. & Gentine, P. Large and projected strengthening moisture limitation on end-of-season photosynthesis. *Proc. Natl Acad. Sci. USA* **117**, 9216–9222 (2020).

54. Bongers, F. J., Olmo, M., Lopez-Iglesias, B., Anten, N. P. R. & Villar, R. Drought responses, phenotypic plasticity and survival of Mediterranean species in two different microclimatic sites. *Plant Biol.* **19**, 386–395 (2017).

55. Nicotra, A. B. et al. Plant phenotypic plasticity in a changing climate. *Trends Plant Sci.* **15**, 684–692 (2010).

56. Chaves, M. M., Maroco, J. P. & Pereira, J. S. Understanding plant responses to drought—from genes to the whole plant. *Funct. Plant Biol.* **30**, 239–264 (2003).

57. Gupta, A., Rico-Medina, A. & Caño-Delgado, A. I. The physiology of plant responses to drought. *Science* **368**, 266–269 (2020).

58. Stirling, E., Fitzpatrick, R. W. & Mosley, L. M. Drought effects on wet soils in inland wetlands and peatlands. *Earth Sci. Rev.* **210**, 103387 (2020).

59. Beck, H. E. et al. Present and future Köppen-Geiger climate classification maps at 1-km resolution. *Sci. Data* **5**, 180214 (2018).

60. Köppen, W. The thermal zones of the Earth according to the duration of hot, moderate and cold periods and to the impact of heat on the organic world. *Meteorol. Z.* **1**, 215–226 (1884).

61. Kottek, M., Grieser, J., Beck, C., Rudolf, B. & Rubel, F. World map of the Köppen-Geiger climate classification updated. *Meteorol. Z.* **15**, 259–263 (2006).

62. Stephenson, N. L. Climatic control of vegetation distribution: the role of the water balance. *Am. Nat.* **135**, 649–670 (1990).

63. Wang, X., Wu, C., Liu, Y., Peñuelas, J. & Peng, J. Earlier leaf senescence dates are constrained by soil moisture. *Glob. Change Biol.* **29**, 1557–1573 (2023).

64. Fu, Z. et al. Atmospheric dryness reduces photosynthesis along a large range of soil water deficits. *Nat. Commun.* **13**, 989 (2022).

65. Zhang, Y., Keenan, T. F. & Zhou, S. Exacerbated drought impacts on global ecosystems due to structural overshoot. *Nat. Ecol. Evol.* **5**, 1490–1498 (2021).

66. Wang, S. et al. Recent global decline of CO_2 fertilization effects on vegetation photosynthesis. *Science* **370**, 1295–1300 (2020).

67. Reinhart, V. et al. Comparison of ESA climate change initiative land cover to CORINE land cover over Eastern Europe and the Baltic States from a regional climate modeling perspective. *Int. J. Appl. Earth Obs. Geoinf.* **94**, 102221 (2021).

68. Beck, H. E. et al. MSWEP V2 global 3-hourly 0.1° precipitation: methodology and quantitative assessment. *Bull. Am. Meteorol. Soc.* **100**, 473–500 (2019).

69. Allen, R. G., Pereira, L. S., Raes, D. & Smith, M. *Crop Evapotranspiration: Guidelines for Computing Crop Water Requirements.* FAO Irrigation and Drainage Paper No. 56 (FAO, 1998).

70. Singer, M. B. et al. Hourly potential evapotranspiration at 0.1° resolution for the global land surface from 1981-present. *Sci. Data* **8**, 224 (2021).

71. Rodell, M. et al. The global land data assimilation system. *Bull. Am. Meteorol. Soc.* **85**, 381–394 (2004).

72. Ferguson, C. R., Wood, E. F. & Vinukollu, R. K. A global intercomparison of modeled and observed land–atmosphere coupling. *J. Hydrometeorol.* **13**, 749–784 (2012).

73. Myneni, R. B., Keeling, C. D., Tucker, C. J., Asrar, G. & Nemani, R. R. Increased plant growth in the northern high latitudes from 1981 to 1991. *Nature* **386**, 698–702 (1997).

74. Badgley, G., Field, C. B. & Berry, J. A. Canopy near-infrared reflectance and terrestrial photosynthesis. *Sci. Adv.* **3**, e1602244 (2017).

75. Jin, H. & Eklundh, L. A physically based vegetation index for improved monitoring of plant phenology. *Remote Sens. Environ.* **152**, 512–525 (2014).

76. Jiao, W. et al. Observed increasing water constraint on vegetation growth over the last three decades. *Nat. Commun.* **12**, 3777 (2021).

77. Zhang, Y., Joiner, J., Alemohammad, S. H., Zhou, S. & Gentine, P. A global spatially contiguous solar-induced fluorescence (CSIF) dataset using neural networks. *Biogeosciences* **15**, 5779–5800 (2018).

78. Joiner, J. & Yoshida., Y. *Global MODIS and FLUXNET-derived Daily Gross Primary Production, V2.* https://doi.org/10.3334/ORNLDAAC/1835 (ORNL DAAC, 2021).

79. Jönsson, P. & Eklundh, L. TIMESAT—a program for analyzing time-series of satellite sensor data. *Comput. Geosci.* **30**, 833–845 (2004).

80. Jin, H. et al. New satellite-based estimates show significant trends in spring phenology and complex sensitivities to temperature and precipitation at northern European latitudes. *Int. J. Biometeorol.* **63**, 763–775 (2019).

81. Granger, C. W. J. & Newbold, P. Spurious regressions in econometrics. *J. Econom.* **2**, 111–120 (1974).

82. Maaten, L. V. D. & Hinton, G. Visualizing data using t-SNE. *J. Mach. Learn. Res.* **9**, 2579–2605 (2008).

83. Enders, W. *Applied Econometric Time Series* 4th edn, 485 (Wiley, 2014).

84. Hoerl, A. E., Kannard, R. W. & Baldwin, K. F. Ridge regression: some simulations. *Commun. Stat.* **4**, 105–123 (1975).

Competing interests

The authors declare no competing interests.

Additional information

Supplementary information The online version contains supplementary material available at https://doi.org/10.1038/s43247-023-00960-w.

Correspondence and requests for materials should be addressed to Hongxiao Jin.

Peer review information *Communications Earth & Environment* thanks Wenzhe Jiao and the other anonymous reviewer(s) for their contribution to the peer review of this work. Primary handling editors: Erika Buscardo, Heike Langenberg. A peer review file is available.

Reprints and permission information is available at http://www.nature.com/reprints

Publisher's note Springer Nature remains neutral with regard to jurisdictional claims in published maps and institutional affiliations.